AXIAL CRUSHING OF PRISMATIC MULTI-CORNER METAL COLUMNS CONSIDERING PLASTIC HARDENING AND CURVATURE

A. Malekshahi* K. H. Shirazi M. Shishehsaz

Department of Mechanical Engineering
Shahid Chamran University of Ahvaz
Ahvaz, Iran

ABSTRACT

In this paper, progressive crushing of prismatic multi-corner thin walled metal tubes under quasi-static axial load is investigated in detail. The novelty of the paper is mainly in considering strain hardening effect during plastic deformation instead of rigid plastic model and also the effect of curvature in forming the folds instead of plastic hinges. For this purpose, a new geometric model based on FEM and experimental observations is used which is capable of being adapted with new crushing configurations during crushing. Based on this model, the instantaneous energy associated with plastic deformation of different regions are calculated and finally by summing all energies and using minimum absorbed energy, mean crushing force and collapse parameters are determined. To evaluate the results, a detailed finite element study using ABAQUS and LS-Dyna solver is conducted on some regular polygonal mild steel tubes under axial crushing. Comparing the results of the new theoretical approach with FEM results show very good capability of that in predicting collapse behavior of these structures.

Keywords: Thin-walled metal tubes, Linear hardening, Axial crushing.

1. INTRODUCTION

Thin walled metal structures, because of their high strength-to-weight ratio, have numerous engineering applications in various fields such as civil engineering as metal components in frames and structures for carrying load or transportation applications such as crashworthiness and absorbing impact in aircrafts, ships, road and rail vehicles. Before designing these structures, it is important to analyze simple geometries in the shortest time and most efficient way possible. One of the main problems in this field is the crushing or collapse analysis of thin walled metal columns with different section shapes to evaluate energy absorption capacity in axial quasi-static loading. Crushing performance of thin walled metal sections has not been investigated enough because of two main reasons; firstly, most of the structures are designed to perform in elastic range loading conditions and beyond that they lose their efficiency and secondly, if there is any application including large deformation of the structure such as energy absorption or crashworthiness, the researchers try not to entangle themselves in complexity of the problem because large deformations include very complicated and uncertain nonlinearities which make the solution out of reach and suspicious. The only present way to handle the problem is to use finite element codes like LS-Dyna solver which is also very slow and computationally expensive even for simple geometries.

Axial collapse of thin-walled metal columns have been addressed by different researchers from different aspects. Alexander [1] presented a theoretical prediction of mean crushing force for thin walled cylindrical metal columns collapsing under quasi-static loading based on a simple model. The first serious analytical study on axial collapse of columns under quasi-static load were carried out by Wierzbicki and Abramowicz [2], Wierzbicki [3], Hayduk and Wierzbicki [4]. They used a theory called Super Folding Element (SFE), an alternative method which instead of solving complicated differential equations governing shell deformation, calculates the energy absorbed in certain areas of the metal plate which undergoes large plastic deformation. By means of this method and selecting an element and suggesting some collapse modes based on experimental observations, they derived relations for absorbed energy during collapse. Their predictions had acceptable, fair or relatively good agreement with experimental results [2-4]. White *et al*. [5] and Najafi and Rais-Rohani [6] used this method to predict mean crushing force for different geometries. Abramowicz and Wierzbicki [7] later on made some predictions for mean crushing force of prismatic thin-walled metal columns based on combining previous collapse modes i.e. quasi-extensional

* Corresponding author (a-malekshahi@phdstu.scu.ac.ir.)

DOI : 10.1017/jmech.2018.2

and extensional. Abramowicz [8] used a method for determining effective crushing distance and its effect on mean force of axially compressed thin-walled metal columns. Tarigopula *et al*. [9] and Langseth and Hopperstad [10] investigated quasi-static axial collapse of thin walled columns from different points of view using similar approach and compared the results with experimental tests.

There are some new theoretical and experimental studies which have used the conventional plastic hinge and perfect plastic material model in crushing. Song *et al*. [11] presented a new model to obtain a relationship between the progressive collapse of an axially loaded tube and the initial buckling of its windowed counterpart. Zhang and Zhang [12-18] in multiple papers investigated crushing behavior of different geometries from several aspects such as experimental and numerical investigation on crush resistance of polygonal columns, axial crushing of multi-cells, Energy absorption of multi-cell stub columns under axial compression and Axial crushing of circular multi-cell columns. Hao *et al.* [19] investigated progressive buckling and energy absorption of the sinusoidal corrugated tube subjected to axial crushing based on SFE theory. Hong *et al*. [20] investigated energy absorption of multi-cell tubes with triangular and kagome lattices under quasi-static axial compression based on experimental tests.

The crushing of structures are important from two aspects firstly the load carrying capacity under axial compression i.e. peak load and secondly absorbed energy during crushing. Based on this, in this paper, first a buckling analysis is carried out to estimate ultimate load of buckling. There are two general methods to evaluate ultimate buckling load [21]; effective width and direct strength methods. The effective width theory has been proved to be more effective so here it is used to estimate ultimate load and since in buckling the material is assumed elastic the energy of buckling is also added to the energy of crushing later on. Second the energy absorbed during crushing is determined by tracking instantaneous deformation mode of a corner element by dividing it to different energy absorbing regions and adding up their energies. At last, using minimum absorbed energy, the mean crushing force and collapse parameters are determined. To evaluate the efficiency of this model, a detailed finite element study using ABAQUS and LS-Dyna solver is conducted on some regular polygonal mild steel tubes under axial crushing. Comparing the results of the new theoretical approach with FEM results show very good capability of that in predicting collapse behavior of these structures.

2. THEORETICAL APPROACH

2.1 Buckling Analysis

Winter and Pian [21] using effective width method and calibration with experimental data, showed that the ultimate local buckling load for a thin-walled column is as follows:

$$P_{ult} = N\sigma_y t \begin{cases} \frac{1}{\lambda}\left(1-\frac{0.218}{\lambda}\right)C & \lambda > 0.673 \\ C & \lambda < 0.673 \end{cases} \quad (1)$$

Where N is the number of polygonal tube corners, σ_y is the material yield strength, t is the thickness, C is the width and λ is the square root of material yield strength to critical stress ratio defined as follows:

$$\lambda = \sqrt{\frac{\sigma_y}{\sigma_{cr}}} \quad (2)$$

σ_{cr} is the critical buckling stress which is obtained from eigenvalue analysis for one plate as follows:

$$\sigma_{cr} = \frac{k_c \pi^2 E}{12(1-\upsilon^2)}\left(\frac{t}{C}\right)^2 \quad (3)$$

Where k_c, E and v are the buckling coefficient, Young modulus and poisson's ratio respectively. By assuming a linear load-displacement curve until collapse and all plates having simply supported boundary conditions ($k_c \cong 4$) irrespective of connecting angle between plates according to FEM results, the absorbed elastic energy before collapse is estimated as:

$$E_0 = \frac{P_{ult} L^2}{2EA_g} \quad (4)$$

Where L is the length of column, and A_g is the gross cross section area of the tube. It is assumed that elastic energy is absorbed during buckling and in crushing, as it will be seen later, material is assumed rigid-linear hardening. Therefore energy E_0 will be added to plastic energy obtained in the following section.

2.2 Crushing Analysis

In post-buckling regime, the column undergoes large plastic deformation and the energy is absorbed through large plastic deformation. A corner element cut out from the column sidewalls with geometrical parameters shown in Fig. 1(a) is often used as the base element in collapse analysis which was suggested by Abramowicz and Wierzbicki [1]. We also use this flattened mechanism for describing the relation between geometric parameters. According to Fig. 1(b):

$$\beta(\alpha) = \tan^{-1}\left(\frac{\tan\alpha}{\sin\psi_0}\right) \quad (5)$$

$$\gamma(\alpha) = \tan^{-1}\left(\frac{\tan\psi_0}{\sin\alpha}\right) \quad (6)$$

According to this model energy is absorbed in concentrated regions and the remaining parts have rigid motion so this model doesn't capture the curvature and material hardening effects. Here we are going to offer a new model based on the old one that includes the curvature of the walls and strain hardening effects. By considering a linear strain hardening model for plastic

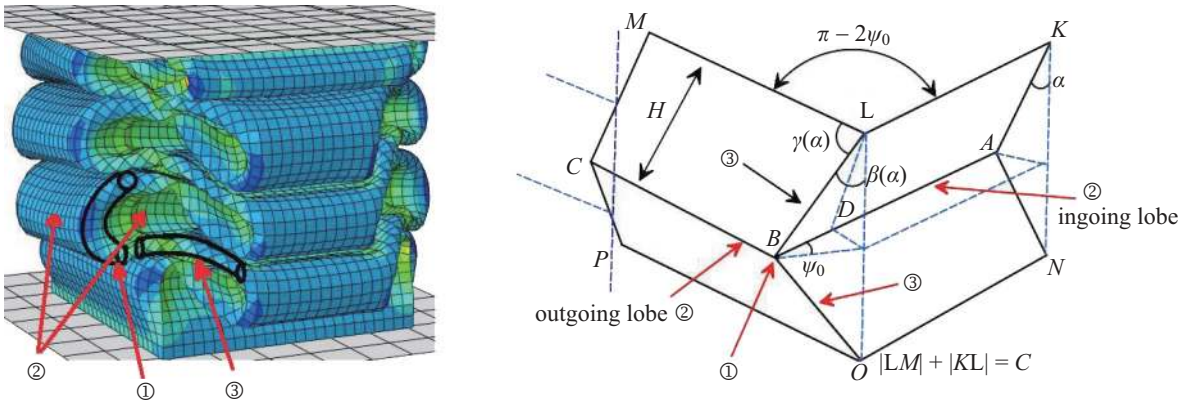

(a) (b)

Fig. 1 (a) quasi-extensional collapse mode including regions under plastic deformations (b) a simple corner element model

deformation, effective stress-strain relation from uniaxial tensile test is obtained as follows:

$$\sigma(\varepsilon) = \sigma_y + E_T \varepsilon \tag{7}$$

Where σ and ε are effective stress and strain respectively. According to Levy-Mises flow rule, principal stress components for plane stress condition [2, 3]:

$$\{\sigma_1, \sigma_2, \sigma_3\} = \left\{ \frac{\bar{\sigma}}{\sqrt{3}} \frac{2\dot{\varepsilon}_1 + \dot{\varepsilon}_2}{\sqrt{\dot{\varepsilon}_1^2 + \dot{\varepsilon}_1^2 + \dot{\varepsilon}_1\dot{\varepsilon}_2}}, \frac{\bar{\sigma}}{\sqrt{3}} \frac{2\dot{\varepsilon}_2 + \dot{\varepsilon}_1}{\sqrt{\dot{\varepsilon}_1^2 + \dot{\varepsilon}_1^2 + \dot{\varepsilon}_1\dot{\varepsilon}_2}}, 0 \right\} \tag{8}$$

Where $\bar{\sigma}$ is Von-Mises equivalent stress based on new plastic yield surface and is related to equivalent strain $\bar{\varepsilon}$ as follows:

$$\bar{\sigma} = \sigma_y + E_T \bar{\varepsilon} \tag{9}$$

By assuming incompressibility condition for the plate, $\bar{\varepsilon}$ is obtained as follows [2, 3]:

$$\bar{\varepsilon} = \sqrt{\frac{4}{3}\left(\varepsilon_1^2 + \varepsilon_2^2 + \varepsilon_1\varepsilon_2\right)} \tag{10}$$

In a simple analysis $\bar{\sigma}$ may be replaced by σ_y. Also in plane strain condition where ε_2 could be neglected compared to ε_1:

$$\bar{\varepsilon} = \frac{2}{\sqrt{3}} \varepsilon_1 \tag{11}$$

Energy absorption rate in shell and plates in general form and in case of neglecting shear effects could be written as:

$$\dot{E} = \iint_A (M_{\alpha\beta}\dot{\kappa}_{\alpha\beta} + N_{\alpha\beta}\dot{\lambda}_{\alpha\beta}) dA = \iint_A \sum_{i=1}^{2} (M_i\dot{\kappa}_i + N_i\dot{\lambda}_i) dA \tag{12}$$

Where $M_{\alpha\beta}$ and $N_{\alpha\beta}$ are generalized in-plane components of moments and forces respectively. $\dot{\kappa}_{\alpha\beta}$ and $\dot{\lambda}_{\alpha\beta}$ are components of rate of curvature and extension tensors respectively. Index i denotes corresponding principal value in ith direction. Equations (7-12) are the governing constitutive equations used here to derive absorbed energy i.e. according to geometry, the strain, curvature and rate of strain and curvature are obtained then the stress then in-plane moments and forces and finally energy is determined.

To illustrate the method used by this paper lets first look at Fig. 2. As it is shown in Fig. 2(a), there are two types of folds in a typically crushed structure named here as ingoing and outgoing lobes. As modelled in Fig. 2(b), according to kinematic constraints, at final state of crushing, the outgoing lobes are two times bigger than ingoing ones because the inner space of the tube should accommodate the ingoing lobes from all sides while the outgoing lobes are free to go outside. This model could also consider the effective crushing length as a function of geometric parameters of the tube. Also by looking at the top view of the crushed tube shown in Fig. 2(c), the length of the ingoing folds increase and outgoing folds decrease which is modelled as shown in Fig. 2(d).

Next, the interaction of the walls are considered. By reviewing Figs. 1 and 2, the overall surface of the tube could be divided into 3 different zones; sidewall plates which separately undergo ingoing and outgoing bending deformation (zone denoted by (2) in Fig. 1), rolling of the corner edges (zone denoted by (3)) and extension in a torus shape surface (zone denoted by (1)). Therefore there are three different radii i.e. ingoing radius, outgoing radius and rolling radius which are all related to each other and shown in Fig. 3.

First, the toroidal surface is considered. According to Fig. 3(a) and Fig. 3(b), the torus is connecting the inner and outer radii which have different bending directions. Wierzbicki [1] stated in his work that although this area is small compared to all the tube surface, but due to extention, it accounts for almost 35 percent of the

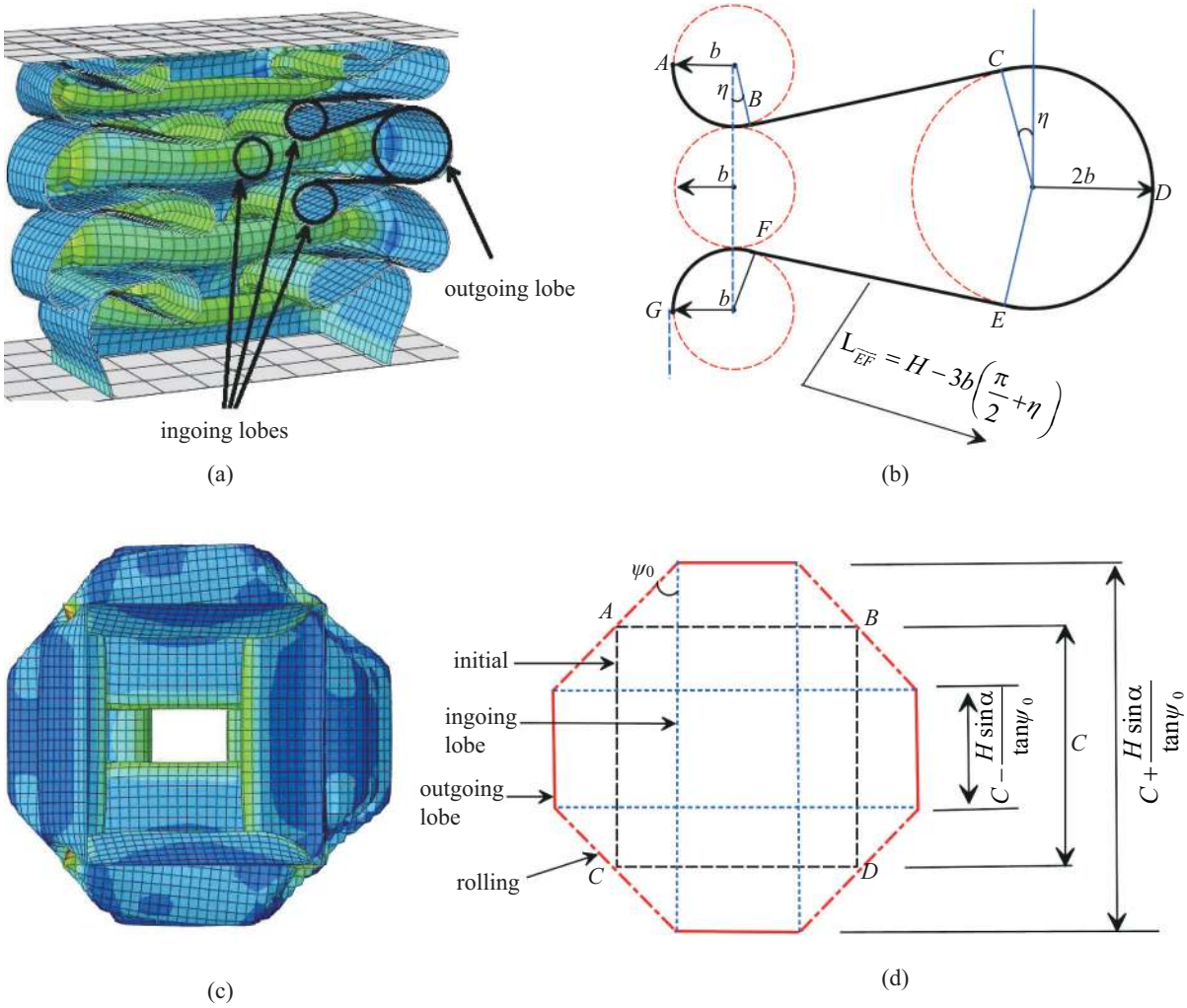

Fig. 2 (a) inner side view showing ingoing and outgoing lobes (b) modelling the curvature of folds (c) top view of the crushing tube (d) a model showing progressing the ingoing and outgoing lobes.

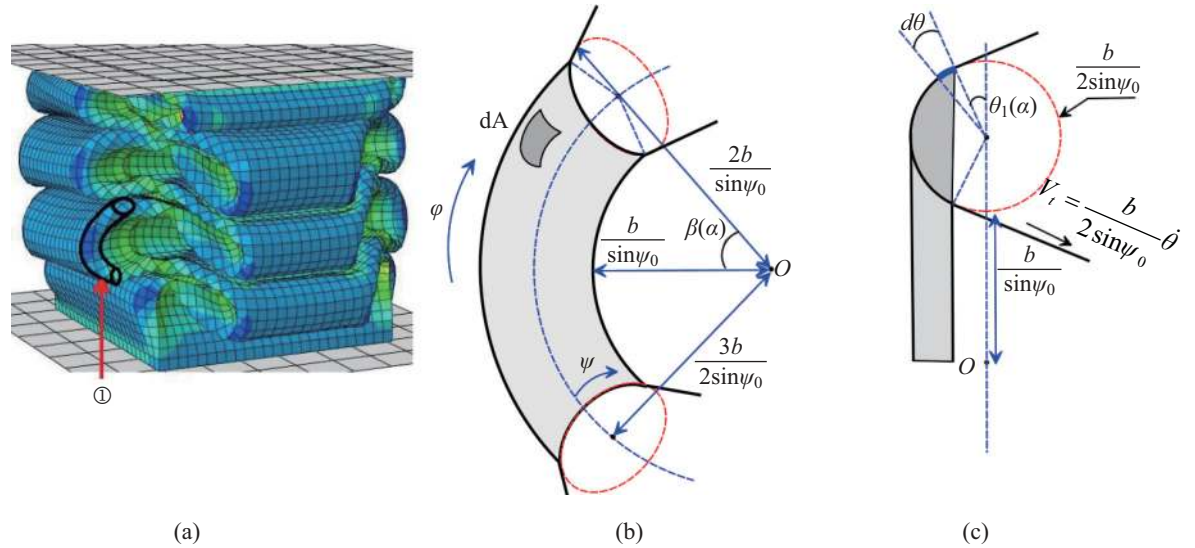

Fig. 3 (a) different regions in absorbing energy (b) geometry of toroid surface (c) section of the torus.

energy based on his analysis. Here we assume that the torus is growing on a predefined surface with known radius and curvatures.

By assuming a local coordinate system in meridian, circumferential and thickness directions respectively denoted by $\{\theta,\varphi,y\}$ as principal directions, the bending radius in circumferential direction:

$$r = a_1 + b_1\cos\theta = \frac{b}{2\sin\psi_0}(3+\cos\theta) \tag{13}$$

Where a_1 and b_1 are major and minor radii of torus surface respectively. The components of strain and strain rate in each point are:

$$\{\varepsilon_\varphi,\varepsilon_\theta,\dot{\varepsilon}_\varphi,\dot{\varepsilon}_\theta\} = \left\{\frac{b_1}{a_1}\cos\theta,\frac{y}{b_1},-\frac{b_1}{a_1}\dot{\theta}\sin\theta,0\right\} \tag{14}$$

Where y is the distance from middle surface of the plate. The components of curvature and rate of curvature at each point:

$$\{\kappa_\varphi,\kappa_\theta,\dot{\kappa}_\varphi,\dot{\kappa}_\theta\} = \left\{\frac{1}{r},\frac{1}{b_1},\frac{b_1\dot{\theta}\sin\theta}{r^2},0\right\} \tag{15}$$

$b_1\dot{\theta}$ is the tangential velocity of the metal passing over the torus in θ direction and according to Fig. 1(b) could be stated as:

$$b_1\dot{\theta} = V_t = \frac{H\cos\alpha}{2\tan\psi_0}d\alpha \tag{16}$$

Substituting strain components in Eq. (12) into Eq. (8), the components of the stress in each direction is obtained as follows:

$$\sigma_\varphi = \frac{2}{\sqrt{3}}\bar{\sigma};\quad \sigma_\theta = \frac{1}{\sqrt{3}}\bar{\sigma} \tag{17}$$

And by substituting Eq. (14) into Eq. (8) and then back into Eq. (7):

$$\sigma_\varphi = \frac{2}{\sqrt{3}}\left(\sigma_y + E_T\bar{\varepsilon}\right),\quad \sigma_\theta = \frac{\sigma_\varphi}{2} \tag{18}$$

In which $\bar{\varepsilon}_\theta$, based on Eq. (10) and assuming mean value for ε_θ across thickness equals:

$$\bar{\varepsilon} = \frac{2}{\sqrt{3}}\sqrt{\frac{1}{9}\cos^2\theta + \frac{t^2}{b^2}\sin^2\psi_0 + \frac{t}{3b}\cos\theta\sin\psi_0} \tag{19}$$

Assuming a sector area in a cross section as shown in Fig. 3(c) and calculating the moment and extension:

$$M_\varphi = 2\int_0^{\frac{t}{2}}\sigma_\varphi y b d\theta = \left(\frac{1}{4}\sigma_\varphi t^2\right);\quad N_\varphi = \sigma_\varphi t \tag{20}$$

By substituting Eq. (20) into Eq. (12) and because of symmetry:

$$\dot{E}_1 = 4\int_0^{\beta(\alpha)}\int_{\theta_1}^{\frac{\pi}{2}}\left\{\left(\frac{1}{4}\sigma_\varphi t^2\right)\dot{\kappa}_\varphi + \left(\sigma_\varphi t\right)\dot{\lambda}_\varphi\right\}b_1 d\theta r d\varphi \tag{21}$$

The first term inside Eq. (21) is the contribution of bending and by comparing with second term which is the contribution of extension could be neglected because thickness is much smaller than each radius [2]. By substituting Eq. (19) into Eq. (21) and performing the integral, the energy absorbed by the torus up to the current configuration α is:

$$E_1(\alpha) = \frac{4Hb_1t}{\sqrt{3}\tan\psi_0}\left\{\sigma_y I_1 + E_T I_2\right\} \tag{22}$$

In which I_1 and I_2:

$$I_1 = \int_0^\alpha \beta(\alpha)\cos\alpha\cos\theta_1 d\alpha \tag{23}$$

$$I_2 = \int_0^\alpha \left\{\begin{array}{l} \beta(\alpha)\cos\alpha\left\{\frac{1}{12}\left(2\cos\theta_1 + \frac{3t\sin\psi_0}{b}\right)\right. \\ \left.\sqrt{\cos^2\theta_1 + \left(\frac{3t\sin\psi_0}{b}\right)^2 + \frac{3t\sin\psi_0}{b}\cos\theta_1}\right. \\ +\frac{1}{8}\left(\frac{3t\sin\psi_0}{b}\right)^2\ln\left(\frac{3t\sin\psi_0}{2b} + \cos\theta_1 + \right. \\ \left.\sqrt{\cos^2\theta_1 + \left(\frac{3t\sin\psi_0}{b}\right)^2 + \frac{3t\sin\psi_0}{b}\cos\theta_1}\right) \\ -\frac{1}{12}\left(\frac{3t\sin\psi_0}{b}\right)^2 - \frac{1}{8}\left(\frac{3t\sin\psi_0}{b}\right)^2\ln\left(\frac{9t\sin\psi_0}{b}\right)\end{array}\right\} \tag{24}$$

Since there are two torus surfaces in a crushing wavelength ($2H$) the energy $E_1(\alpha)$ must be doubled to give the total absorbed energy. According to Fig. 3(c), $2\theta_1$ is the angle between two adjacent plates and is a function of α as:

$$\cos 2\theta_1 = 1 - 2\cos^2\alpha\cos^2\psi_0 \tag{25}$$

Integrals (23) and (24) should be evaluated numerically to give absorbed energy at each time α.

Next, the energy absorbed by horizontal ingoing and outgoing folds shown in Fig. 2 is investigated. For this purpose, since the history of forming the lobes is unknown, it is assumed that bending strain and curvature in each point are changed linearly from initial undeformed state to the current crushed state so we assume:

$$\left\{\varepsilon^I,\varepsilon^O,\kappa^I,\kappa^O\right\} = \left\{\frac{\alpha y}{b\alpha_f},\frac{\alpha y}{2b\alpha_f},\frac{\alpha}{b\alpha_f},\frac{\alpha}{2b\alpha_f}\right\} \tag{26}$$

Since the extension rate in direction perpendicular to bending is neglected, the plane strain condition is assumed and the stress at each instance and at each point through thickness for ingoing and outgoing folds are:

$$\sigma^I = \frac{2}{\sqrt{3}}\left(\sigma_y + \frac{2E_T}{\sqrt{3}}\frac{\alpha y}{b\alpha_f}\right);\quad \sigma^O = \frac{2}{\sqrt{3}}\left(\sigma_y + \frac{E_T}{\sqrt{3}}\frac{\alpha y}{b\alpha_f}\right) \tag{27}$$

Therefore the corresponding moments are obtained as follows:

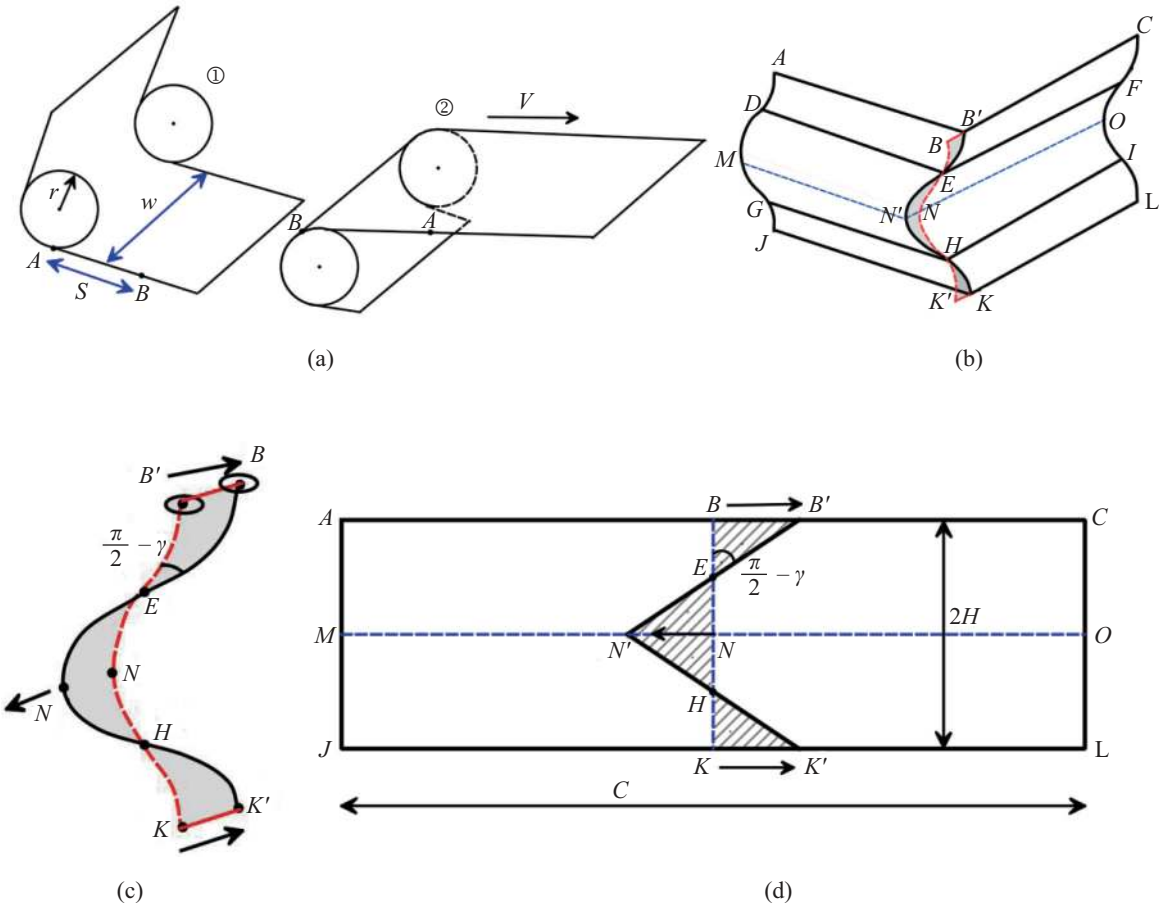

Fig. 4 (a) rolling of a sheet metal (b) rolling region in the corner element (c) detailed model of rolling (d) a flattened corner element showing region swept by rolling deformation.

$$M^I = 2\int_0^{\frac{t}{2}} \sigma^I y dy = \frac{2}{\sqrt{3}}\left(\frac{1}{4}\sigma_y t^2 + \frac{E_T \alpha t^3}{6\sqrt{3} b\alpha_f}\right);$$

$$M^O = \frac{2}{\sqrt{3}}\left(\frac{1}{4}\sigma_y t^2 + \frac{E_T \alpha t^3}{12\sqrt{3} b\alpha_f}\right) \tag{28}$$

Using Eq. (12) and since there are two complete ingoing and outgoing folds in each wavelength with varying lengths as shown in Fig. 2(d), after integrating, the energy due to forming these folds:

$$E_2(\alpha) = E^I + E^O$$
$$= 4\left\{\int_0^{\alpha} M^I\left(\frac{C}{2} + \frac{H\sin\alpha}{2\tan\psi_0}\right)d\alpha + \int_0^{\alpha} M^O\left(\frac{C}{2} - \frac{H\sin\alpha}{2\tan\psi_0}\right)d\alpha\right\} \tag{29}$$

The third energy is due to rolling. First, suppose the sheet metal in Fig. 4(a) rolling from state 1 to state 2. It is easy to prove that the energy absorbed during this transition is composed of a bending and then unbending of sheet in swept area (*s.w*) and also a pure bending like a hinge from state 1 to state 2. So for the element shown in Fig. 4(b), the corner of the tube rolls and bend from BEHK to B′E′H′K′ as shown in Fig. 4(c). Figure 4(d) shows the flattened form of the rolling corner.

The mean stress in rolling direction for each point through thickness is determined in a similar way:

$$\bar{\sigma}_{rol} = \frac{2}{\sqrt{3}}\left(\sigma_y + \frac{E_T}{\sqrt{3}}\frac{2\sin\psi_0 y}{b}\right) \tag{30}$$

And the corresponding rolling moment:

$$\bar{M}_{rol} = 2\int_0^{\frac{t}{2}} \bar{\sigma}_{rol} y dy = \frac{2}{\sqrt{3}}\left(\frac{1}{4}\sigma_y t^2 + \frac{E_T \sin\psi_0}{12\sqrt{3}}\frac{t^3}{b}\right) \tag{31}$$

The energy is sum of rolling (bending and unbending) and a pure bending:

$$E_3(\alpha) = 2\iint_A \bar{M}_{rol}\left(\frac{2\sin\psi_0}{b}\right)dA$$
$$= 2\bar{M}_{rol}\frac{H^2}{b}\sin\psi_0\cot\gamma(\alpha) + \bar{M}_{rol} H I_3 \tag{32}$$

In which the integral I_3 is:

$$I_3 = 2\int_0^{\alpha}\left(\frac{\pi - 2\psi_0 - 2\theta_1}{\sin\gamma(\alpha)}\right)d\alpha \tag{33}$$

The effective crushing distance ratio according to Fig. 2(b) equals:

$$\delta_{eff} = \frac{H - 2b}{H} = 1 - \frac{2b}{H} \tag{34}$$

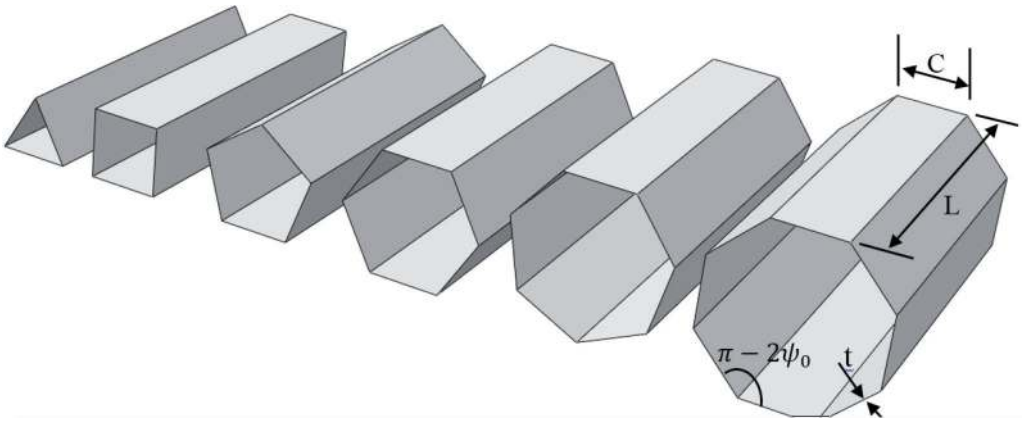

Fig. 5 Different regular polygon thin walled columns with geometric parameters.

2.3 Solution Procedure

In this section, a procedure for solving the equations is proposed. For this purpose first two sets of variables are considered; independent known variables including geometric parameters and mechanical properties denoted by χ:

$$\chi = \{t, C, \psi_0, \sigma_y, E, \nu, E_T\} \tag{35}$$

And dependent unknown variables including collapse variables denoted by ξ:

$$\xi = \{H, b\} \tag{36}$$

The aim is to evaluate ξs and mean crushing force P_m for every given combination of χ. To this aim the total internal energy up to final instance α_f, which is the sum of derived energies should be equal to external work W_{ext} as follows:

$$P_m(\chi, \xi) = \frac{\sum_{i=0}^{3} E_i(\alpha_f)}{2H\delta_{eff}} \tag{37}$$

α_f based on Fig. 2(b) equals $\frac{\pi}{2} + \eta$. For equal ingoing and outgoing of folds η = 0.21 or could be even neglected. Now using minimum value of $P_m(\chi,\xi)$ with respect to ξ:

$$\frac{\partial P_m(\chi, \xi)}{\partial \xi} = 0 \tag{38}$$

Equation (38) consists of two nonlinear algebraic equation which should be solved numerically for each combination of χ to give a point for ξ. By repeating this procedure for each χ, different ξs are obtained. In this way it is possible to plot variation of ξ and mean force P_m for different combination of input parameters χ.

3. FEM MODELLING AND SIMULATION

In this section, the procedure of modelling metal polygon tubes is illustrated. First the tubes are modelled in a CAD software as shown in Fig. 5 then they are submitted for buckling analysis in ABAQUS to obtain ultimate buckling load sometimes known as load carrying capacity under quasi-static axial load.

In the remaining of the paper, to avoid multiple number of simulations and to save time, only the results of triangular, square and hexagonal tubes are considered for validation of theoretical approach. Also we use eight different aspect ratios $\frac{t}{C}$ for each tube as enough by changing only thickness from 0.5 mm to 1.6 mm. The width C is chosen as 50 mm and constant. Length of all tubes denoted by L is chosen 250 mm. To initiate crushing in so called quasi-extensional mode, the tubes must have imperfections. A real tube even with best tolerances has geometric imperfections. There are two ways of embedding imperfections into tubes; one way is inserting crushing initiators artificially such as grooves which is not natural and just used for energy absorption purposes. The other way which is more realistic is to embed imperfections naturally via buckling mode shapes, To this aim, first a linear buckling analysis is conducted in ABAQUS to capture some enough modes, here the first three buckling modes are used. then by combining these mode shapes by a small amplitude, here 0.03 of thickness, the imperfect geometry is generated which is then submitted for nonlinear Static Riks analysis to determine ultimate buckling load. The new geometry with imperfections is then imported into LS-Dyna for axial crushing. Figure 6 shows the first mode shape of each tube. Static Riks analysis in ABAQUS uses arc length method which is a nonlinear analysis to converge to an ultimate buckling load in a stability problem such as axial buckling. The reason for using two different software i.e. buckling in ABAQUS then crushing in LS-Dyna is capabilities of each software in simulation of related analysis. Static Riks analysis doesn't exist in LS-Dyna as it is in ABAQUS and crushing simulation ability in LS-Dyna is more fast and easy to implement compared to ABAQUS.

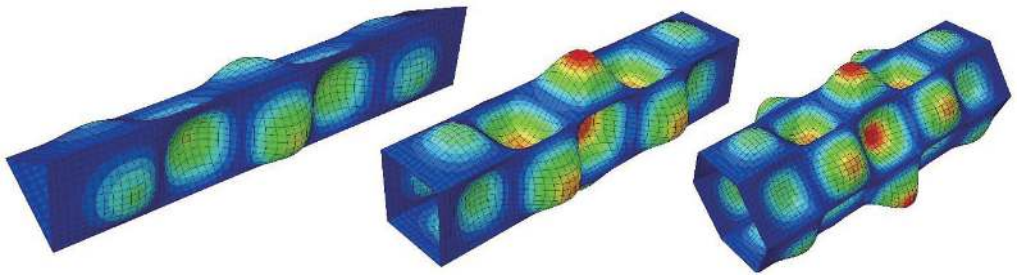

Fig. 6 Linear buckling of the tubes showing first shape mode and mesh size.

Table 1 Mechanical and geometric properties of thin-walled tubes used in this study

Mechanical properties of AISI1020 alloy							Dimensions (geometric parameters)	
E (GPa)	σ_y (MPa)	ν	σ_u (MPa)	K (MPa)	n	ε_u	L (mm)	C/t
207	345	0.29	442	500	0.1	0.3	250	Variable

Table 2 FEM and the current theoretical approach ultimate load and mean crushing force

	Thickness (mm)	0.5	0.6	0.7	0.8	0.9	1	1.3	1.6
Hexagon Tube ($N=6$)	Analytic ultimate load (KN)	23.31	31.82	41.76	54.80	70.73	91.04	134.70	166.60
	Analytic mean crushing force (KN)	10.30	14.22	18.41	23.45	28.67	34.64	54.93	79.14
	FEM ultimate load (KN)	22.25	31.30	41.58	52.98	66.41	81.35	125.72	165.63
	FEM mean crushing force (KN)	9.80	13.47	17.31	22.20	27.37	33.84	53.44	77.83
Square Tube ($N=4$)	Analytic ultimate load (KN)	15.54	21.16	28.11	36.49	47.09	60.58	89.78	111.11
	Analytic mean crushing force (KN)	5.06	7.38	9.60	12.08	14.94	17.91	28.30	40.21
	FEM ultimate load (KN)	14.52	20.43	27.16	34.63	42.76	51.47	80.28	110.40
	FEM mean crushing force (KN)	5.40	7.85	9.90	12.40	15.10	18.23	27.78	38.94
Triangle Tube ($N=3$)	Analytic ultimate load (KN)	12.01	17.08	22.42	30.65	39.77	49.73	66.16	82.51
	Analytic mean crushing force (KN)	2.71	3.93	5.08	6.42	7.81	9.42	14.91	21.31
	FEM ultimate load (KN)	11.90	16.71	22.14	28.15	34.64	41.55	64.07	82.80
	FEM mean crushing force (KN)	2.78	3.78	6.55	7.99	9.18	10.06	14.77	21.17

Shell elements with 5 integration points through thickness, mild steel carbon steel alloy AISI1020 with properties given in Table 1 and 4 mm mesh size are chosen. The boundary condition in lower edges are clamped in all directions.

A rigid plate with friction coefficient 0.2 compresses the tube in axial direction. Afterwards, for crushing analysis, the imperfect tubes are imported into LS-Dyna software for preprocessing operation such as assigning material, meshing, boundary, load and initial conditions and so on. Material model number 24 i.e. 24_MAT_PIECEWISE_LINEAR_PLASTICITY with properties in Table 2. In order to model hardening in FEM simulation a power law strain hardening formula also known as Ludwik's formula which is a realistic model is used which is stated as follows:

$$\sigma = K\varepsilon^n \tag{39}$$

K and n are plastic stiffness and power hardening which for Alloy AISI1020 are determined by curve-fitting Eq. (39) on experimental data. These values are already determined and given in Table 1. In LS-Dyna the values of plastic stress is calculated for different strains up to ultimate strain ε_u using Eq. (39) point by point and entered into the related keyword. Since we have used a linear hardening model instead of a power hardening in our analytic approach, it is necessary to determine hardening modulus E_T in Eq. (9) based on data in Table 1. The relation is as follows:

$$E_T = \frac{\sigma_u - \sigma_y}{\varepsilon_u} \tag{40}$$

ε_u is the plastic strain corresponding to ultimate stress σ_u. For regular polygonal shapes there is a relation between number of corners N and internal angle of each corner $\pi - 2\psi_0$ so that based on our model:

$$\psi_0 = \frac{\pi}{N} \tag{41}$$

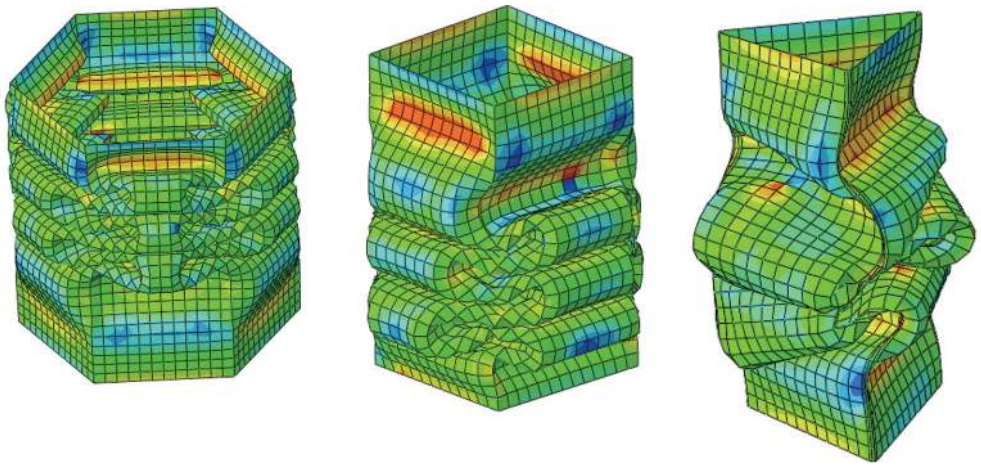

Fig. 7 Crushed tubes modelled in LS-Dyna.

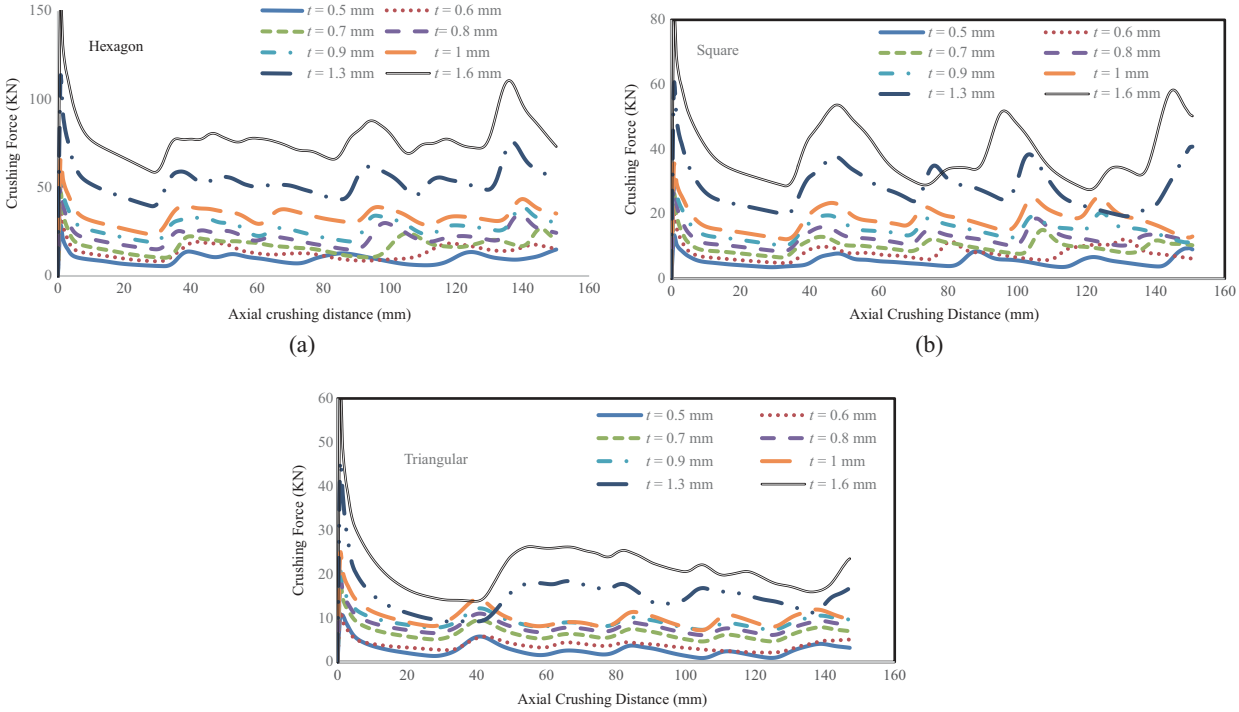

Fig. 8 Crushing force vs. axial displacement for hexagonal, square and triangular tubes.

For shell elements, formulation number 2 i.e. Belytschko-Tsay SECTION_SHELL is used. Zero translational boundary conditions are used for all lower edges. AUTOMATIC_SINGLE_SURFACE contact type is used for shell self-contact with friction coefficient 0.2. RIGIDWALL_GEOMETRIC_FLAT_MOTION Keyword is used to model the rigid plate crushing the tube axially with predefined 150 mm crushing distance. Since LS-Dyna solves the equations using explicit time increments, to simulate a quasi-static load condition, the rigidwall compresses the tube with a low constant velocity of 1.5 m/s. This is done by putting CONTROL_TERMINATION_ENDTIME 0.1 s. The time increment is also chosen 0.001 s to capture enough number of 100 points. After generating the FEM code, it is submitted to LS-Dyna solver for solution. Figure 7 show the crushed state of the tubes. Reducing velocity to less than 1.5 m/s results in no significant change but increases simulation time therefore this velocity is regarded as quasi-static.

4. RESULTS AND DISSCUSION

In this section, the results of finite element modelling including ultimate load obtained from Static Rik's analysis in ABAQUS and mean crushing force in

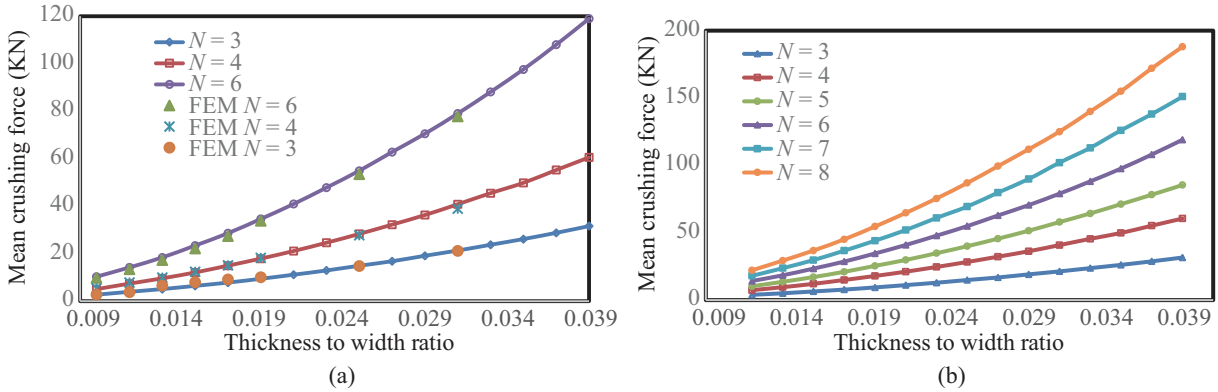

Fig. 9 Mean crushing force vs. thickness/width ratio for different polygonal tubes (a) comparison between theoretical and FEM (b) theoretical approach for all the tubes.

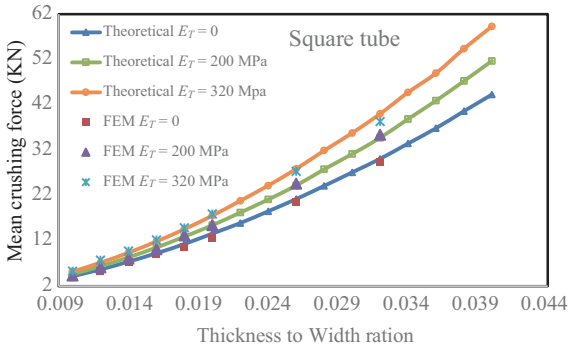

Fig. 10 Mean crushing force vs. thickness/width ratio for square tubes for three different plastic hardening modulus.

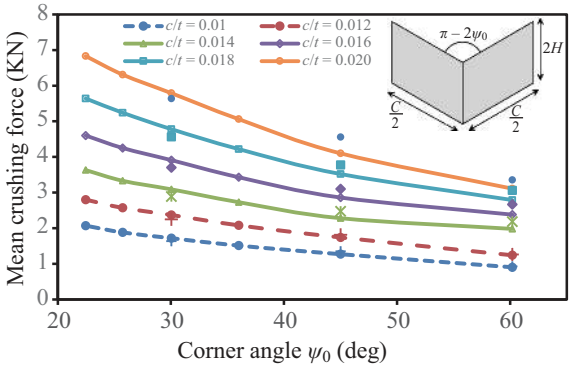

Fig. 11 Variation of Mean crushing force for each corner element by changing angle of the corner element ψ_0 for both FEM (single points) and the current theoretical approach (solid lines).

LS-Dyna solver along with the corresponding values by the current theoretical approach are evaluated and compared with each other. The results are presented in Table 2. As it is seen there is a very good agreement between the two approach. Also, the results of mean crushing force for FEM simulation and the theoretical approach are in good agreement. There is only a slight difference for some triangular tubes which is due to assymetric section of triangular tube.

The force vs. axial displacement curves for different thicknesses of tubes are plotted and shown in Fig. 8(a) to Fig. 8(c). As it is shown there are multiple succeeding peaks associated with progressive folds which shows a complicated irregular behavior but in terms of energy absorption it is possible to assign a mean force for each wavelength. There is only a different behavior for thick triangular tubes because as thickness increases it acts like an Eularian column which undergoes global buckling. Generally larger thickness to width ratios may result in global buckling not axial progressive collapse which is not considered here because in that case the tubes are no longer regarded as thin walled.

The results of mean crushing force vs. thickness to width ratio for FEM and the theoretical approach are shown in Fig. 9(a) which shows very good agreement of the current approach in predicting the absorbed energy. One of the disadvantages of FEM method is that it is computational expensive and needs a lot of time for modelling and preprocessing but analytic approach if there is any is too fast and simple to implement. The results shown in Fig. 9(b) which are the results for other tubes with different thicknesses have been created in a very short time once the code is written, it needs only to run one time to give the mean crushing force for any tube with any shape and size.

Figure 10 shows the effect of plastic hardening on the mean crushing force of square tubes for both FEM and the current theoretical approach. As it can be seen in Fig. 10, the hardening have a mild but significant effect on the mean force. The value of $E_T = 0$ corresponds to a perfectly plastic material. The results of other tubes are similar to Fig. 10.

Figure 11 shows the effect of corner angle $\pi - 2\psi_0$ on mean crushing force for different polygons i.e. from triangular tube with $\psi_0 = \frac{\pi}{3}$ to octagonal tube with $\psi_0 = \frac{3\pi}{4}$. As it can be seen in Fig. 11 the more the corner angle $\pi - 2\psi_0$, the crushing force and absorbed energy will increase this behavior is justified by looking at crushing modes in Fig. 2 and Fig. 3 because for opener angles of the corner element, the ingoing lobes and rolling area which have smaller curvature radii, have

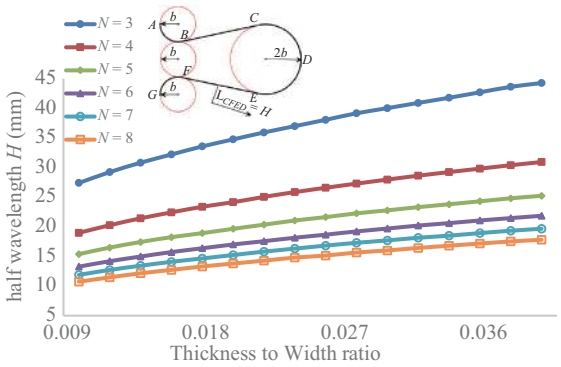

Fig. 12 Crushing wavelength H for different polygon tubes.

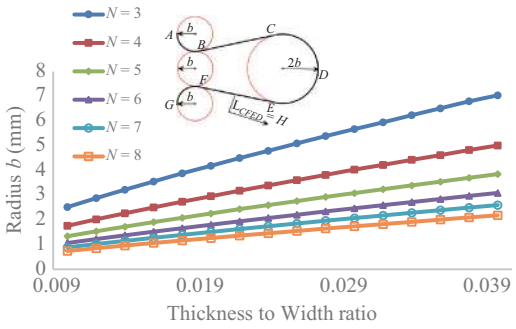

Fig. 13 bending radius b for different polygon tubes.

more contribution in absorbing energy compared to closer angles.

As discussed before collapse variables ξ including half wavelength of crushing H and also the ingoing, outgoing and rolling radii of folds formed during progressive collapse are obtained by the current theoretical approach which are not obtained using FEM. Figures 12 and 13 show the variation of half wavelength H and bending radius b by thickness to width ratio for different polygonal tubes. As it can be seen in these figures, both H and b increase with thickness to width ratio and also these values are decreased for opener corner angles this is also the reason for increasing effective crushing length and mean crushing force for opener angles.

5. CONCLUSIONS

Axial crushing of multi-corner prismatic metal columns undergoing progressive quasi-extensional collapse mode was investigated in detail. Instead of using previous simple models in Refs. [2-8] which assumed that material model as rigid-perfect plastic, in this study hardening of material during plastic deformation was considered also instead of using plastic hinges like previous studies, here the effect of curvature was taken into account. Based on these assumptions and using plastic flow rules governing stress and strain relations for sheet metal, the energies of buckling and post-buckling were derived and finally using minimum absorbed energy the mean crushing force and collapse parameters were determined. A detailed finite element modelling and simulation using ABAQUS for peak loads and LS-Dyna for crushing analysis and obtaining mean crushing force were carried out. Based on the results, there were very good agreement between the theoretical and FEM results which makes it possible to be used as a code as an alternative method for axial crushing of such structures because unlike FEM simulation which takes too much time for preprocessing, post-processing and solution, this method is very fast and gives reliable results for different material and mechanical properties.

ACKNOWLEGEMENTS

The authors would like to show their gratitude to Phd students in Mechanical Engineering Department of Shahid Chamran University especially Mr. S.M. Hosseini and Mr. M.D. Kashkoli who provided insight and expertise that greatly assisted the research

NOMENCLATURE

E	Modulus of elasticity
v	Poisson's ratio
σ_y	Yield strength
σ_u	Ultimate strength
λ	Stress ratio in effective width theory
σ_{cr}	Critical buckling stress
P_{ult}	Ultimate buckling load
A_g	Gross cross section of thin-walled column
ε_u	Ultimate strain
n	Power law hardening coefficient
k_c	Buckling coefficient
E_T	Plastic linear hardening modulus
$\dot{\varepsilon}$	Strain rate
α,β	Indices of in-plane components
t,C,L	Thickness, width and length of the column
$\bar{\sigma},\bar{\varepsilon}$	Von-Mises equivalent stress and strain
ψ_0	Corner angle
E_0	Elastic absorbed energy
E_i	Plastic absorbed energies (i = 1,..,3)
$N_{\alpha\beta}$	Generalized In-plane forces
$M_{\alpha\beta}$	Generalized In-plane moments
$\kappa_{\alpha\beta},\dot{\kappa}_{\alpha\beta}$	Curvature and curvature rate
$\lambda_{\alpha\beta},\dot{\lambda}_{\alpha\beta}$	Extension and extension rate
y	Distance from mid plane

a_1,b_1	Larger and smaller radii of the torus
I_i	Integrals
$\chi = \{t,C,\psi_0,\ldots\}$	Geometric and Mechanical parameters
V_t	Tangential velocity of sheet
σ^I,σ^O	referred to ingoing or outgoing folds
N	Number of corners of polygonal tube
δ_{eff}	Effective crushing length for each fold
$\alpha,\beta,\gamma,\phi,\theta$	Angles of crushing mechanism

REFERENCES

1. Alexander, J., "An Approximate Analysis of the Collapse of Thin Cylindrical Shells under Axial Loading," *The Quarterly Journal of Mechanics and Applied Mathematics*, **13**, pp. 10-15 (1960).
2. Wierzbicki, T. and Abramowicz, W., "On the Crushing Mechanics of Thin-Walled Structures," *Journal of Applied Mechanics*, **50**, pp. 727-734 (1983)
3. Wierzbicki, T., "Crushing Analysis of Metal Honeycombs," *International Journal of Impact Engineering*, **1**, pp. 157-174 (1983).
4. Hayduk, R. J. and Wierzbicki, T., "Extensional Collapse Modes of Structural Members," *Computers & Structures*, **18**, pp. 447-458 (1984).
5. White, M., Jones, N. and Abramowicz, W., "A Theoretical Analysis for the Quasi-Static Axial Crushing of Top-Hat and Double-Hat Thin-Walled Sections," *International Journal of Mechanical Sciences*, **41**, pp. 209-233 (1999).
6. Najafi, A. and Rais-Rohani, M., "Mechanics of Axial Plastic Collapse in Multi-Cell, Multi-Corner Crush Tubes," *Thin-Walled Structures*, **49**, pp. 1-12 (2011).
7. Abramowicz, W. and Wierzbicki, T., "Axial Crushing of Multicorner Sheet Metal Columns," *Journal of Applied Mechanics*, **56**, pp. 113-120 (1989).
8. Abramowicz, W., "The Effective Crushing Distance in Axially Compressed Thin-Walled Metal Columns," *International Journal of Impact Engineering*, **1**, pp. 309-317 (1983).
9. Tarigopula, V. *et al.*, "Axial Crushing of Thin-Walled High-Strength Steel Sections," *International Journal of Impact Engineering*, **32**, pp. 847-882 (2006).
10. Langseth, M. and Hopperstad, O., "Static and Dynamic Axial Crushing of Square Thin-Walled Aluminium Extrusions," *International Journal of Impact Engineering*, **18**, pp. 949-968 (1996).
11. Song, J., Zhou, Y. and Guo, F., "A Relationship between Progressive Collapse and Initial Buckling for Tubular Structures under Axial Loading," *International Journal of Mechanical Sciences*, **75**, pp. 200-211 (2013).
12. Zhang, X. and Zhang, H., "Crush Resistance of Square Tubes with Various Thickness Configurations," *International Journal of Mechanical Sciences*, **107**, pp. 58-68 (2016).
13. Zhang, X. and Huh, H., "Crushing Analysis of Polygonal Columns and Angle Elements," *International Journal of Impact Engineering*, **37**, pp. 441-451 (2010).
14. Zhang, X. and Zhang, H., "Energy Absorption Limit of Plates in Thin-Walled Structures under Compression," *International Journal of Impact Engineering*, **57**, pp. 81-98 (2013).
15. Zhang, X. *et al*., "Energy Absorption of Axially Compressed Thin-Walled Square Tubes with Patterns," *Thin-Walled Structures*, **45**, pp. 737-746 (2007).
16. Zhang, X. and Zhang, H., "Experimental and Numerical Investigation on Crush Resistance of Polygonal Columns and Angle Elements," *Thin-Walled Structures*, **57**, pp. 25-36 (2012).
17. Zhang, X. and Zhang, H., "Numerical and Theoretical Studies on Energy Absorption of Three-Panel Angle Elements," *International Journal of Impact Engineering*, **46**, pp. 23-40 (2012).
18. Zhang, X. and Zhang, H., "Theoretical and Numerical Investigation on the Crush Resistance of Rhombic and Kagome Honeycombs," *Composite Structures*, **96**, pp. 143-152 (2013).
19. Hao, W., Xie, J. and Wang, F., "Theoretical Prediction of the Progressive Buckling and Energy Absorption of the Sinusoidal Corrugated Tube Subjected to Axial Crushing," *Computers & Structures*, **191**, pp. 12-21 (2017).
20. Hong, W. *et al*., "Axial Crushing Behaviors of Multi-Cell Tubes with Triangular Lattices," *International Journal of Impact Engineering*, **63**, pp. 106-117 (2014).
21. Winter, G. and Pian, R., "Crushing Strength of Thin Steel Webs," Cornell University (1946).
22. Mendelson, A., "*Plasticity, Theory and Application*," Macmillan, New York, 367 (1968).
23. Hodge, P. G., "*Plastic Analysis of Structures*," McGraw-Hill, New York, 378 (1959).

(Manuscript received October 7, 2017,
accepted for publication December 14, 2017.)